

# Constraints on granite-related uranium mineralization in the Sanjiu uranium ore field, SE China provided by pyrite mineralogy, major and trace elements, S–He–Ar isotopes

Xu Chen<sup>1,3</sup>  · Xiaodong Liu<sup>1,2</sup> · Jinning Qin<sup>3</sup> · Biguang Jiang<sup>3</sup>

Received: 18 July 2019 / Revised: 9 February 2020 / Accepted: 9 March 2020 / Published online: 18 March 2020  
© Science Press and Institute of Geochemistry, CAS and Springer-Verlag GmbH Germany, part of Springer Nature 2020

**Abstract** The Sanjiu uranium ore field, located in the central of Zhuguangshan granitic batholith, is a newly discovered granite-related uranium ore field in South China. The main sulfide in the ore field is pyrite, which is closely related to uranium mineralization. The textures, major and trace elements, S–He–Ar isotopes compositions of pyrites in ores of different grade were observed and/or analyzed by optical microscope, scanning electron microscope, electron microprobe, laser ablation inductively coupled plasma mass spectrometry, and noble gas mass spectrometer (Helix-SFT). It is observed that these U-related pyrites are generally euhedral–subhedral with dissolution textures, anhedral variety with colloform texture, veinlet and fine particles, and the color of the associated minerals is mostly dark hue, such as purple–black fluorite, dark-red hematite, and dark-green chlorite, etc. The analytical results show that the average compositions of major elements in pyrite are FeS<sub>1.944</sub>. Pyrites are characterized by S-deficiency, low content of Co and Th, and Co/Ni > 1, which indicate that these ores are of low-temperature hydrothermal origin. We found that the higher the grade of ore, the more deficient in S, the more obvious negative

$\delta^{34}\text{S}$ , and the higher REE content (close to U-rich granitic pluton) of pyrite. The S–He–Ar isotopic compositions of various varieties of pyrites indicate that the ore-forming fluids mainly come from crust-derived fluids and mixed with mantle-derived fluids.

**Keywords** Pyrite · In-situ analysis · Noble gas isotope · Granite-related uranium deposit · The Sanjiu uranium ore field

## 1 Introduction

Granite-related uranium (U) deposits belong to one of the 15 types of U deposits in the new International Atomic Energy Agency (IAEA) geological classification. The deposit is closely related to granite (mostly are peraluminous, two-mica granite complexes), and the U mineralization occurs within, at the contact or peripheral to the granite. There are two subtypes of the deposits related to granite, endogranitic deposits within the granite and perigranitic deposits in the adjacent country rocks (IAEA, 2016). The U deposits in China are generally hosted by four types of rocks: granite, volcanic rock, carbonaceous-siliceous-pelitic rocks, and sandstone. The granite-related U deposits in China, contribute 22.9% of identified U resources, which occur mainly in South China (Cai et al. 2015). Zhuguangshan granitic batholith (ZGB), a famous and important granite-related U ore concentration area, located within Taoshan-Zhuguang U metallogenic belt in Southeast China U province (Zhang et al. 2012). The Sanjiu area, between the Lujing and Chengkou U ore fields, is located in the middle of the ZGB. The uranium resources of the Sanjiu area have risen to the level of ore field, due to many uranium deposits discovered over the past decade

**Electronic supplementary material** The online version of this article (<https://doi.org/10.1007/s11631-020-00411-9>) contains supplementary material, which is available to authorized users.

✉ Xu Chen  
373193083@qq.com

<sup>1</sup> State Key Laboratory of Nuclear Resources and Environment, East China University of Technology, Nanchang 330013, China

<sup>2</sup> Jiujiang University, Jiujiang 332005, China

<sup>3</sup> The 306 Team of Hunan Nuclear Geology, Hengyang 421000, China

(Fig. 1). Previous research in the Sanjiu uranium ore field (SUOF) had been focused on the deposit exploration as metallogenic geological background, strata, granite, ore-controlling fault, U orebody, etc. (Deng et al. 2003; Qin et al. 2003; Huang et al. 2008; Shao et al. 2010; Du et al. 2011, 2012; Fei et al. 2012; Ouyang and Wang, 2013; Lan, 2015; Chen and Zhang 2016; Wang et al. 2016, 2017; Jiang et al. 2017; Lan et al. 2018). In contrast, the mineralogical studies on granite-related uranium mineralization have scarcely been studied, despite the ubiquitous presence of pyrite in granite.

Pyrite ( $\text{FeS}_2$ ), which generally records a significant amount of ore-forming information, is a common and redox-sensitive mineral in endogenetic deposits. Ore deposit research of pyrite generally involves isotopes, major and trace elements, fluid inclusions, which are used to study ore-forming age, ore-forming fluid properties, ore-forming conditions and environment (Hu et al. 1997; Mao et al. 2008; Cook et al. 2009; Yan et al. 2012; Lu et al. 2013; Agangi et al. 2014; Khishgee et al. 2014; Fuchs et al. 2016; Dehnavi et al. 2018). Previous work shows that pyrite is closely associated with granite-related U deposits, due to the sulfur in pyrite acting as a reducing agent in uranium mineralization (Zhao and Shen, 1986; Huang 2000; Fan et al. 2001; Du et al. 2011; Zou et al. 2017; Liu et al. 2018). Therefore, pyrite has been considered one of the important prospecting indicators for granite-related U deposits. S, He, Ar isotopic analysis of minerals such as pyrite had been studied for the genesis and composition of ore-forming fluids in some U deposits, and these studies have shown that the ore-forming fluids are generally of crust-mantle mixed origin (Zhang et al. 2010; Zou et al. 2017; Liu et al. 2018). However, there are also considerable explorations showing that varieties of pyrites in the ore do not indicate U mineralization well. Up to now, it is not clear how pyrite affects or restricts the granite-related U mineralization, especially in morphology, geochemical composition.

Recently, LA-ICP-MS has been widely used in the in-situ analysis of pyrite and other minerals. Compared with traditional analytical techniques, in-situ analysis can help interpret the genesis of hydrothermal deposits more accurately (Large et al. 2009; Ulrich et al. 2011; Zhang et al. 2014a, b; Leng 2017; Liu et al. 2018). In this paper, ore samples containing pyrite were taken from different ore-controlling faults and rocks in the SUOF. The textures, major and trace elements and isotopic compositions of pyrites are studied by means of optical microscopy, scanning electron microscopy (SEM), electron microprobe (EMPA), laser ablation inductively coupled plasma mass spectrometry (LA-ICP-MS), and noble gas mass spectrometer (Helix-SFT). These data may provide valuable information for the ore genesis and further exploration.

**Fig. 1** **a** Geotectonic location map of the ZGB (modified from Mao et al. 2017); **b** schematic map of granitic plutons and U ore fields in central and southern part of the ZGB (modified from Deng et al. 2012); **c** simplified geological map of the SUOF (after Chen et al. 2013)

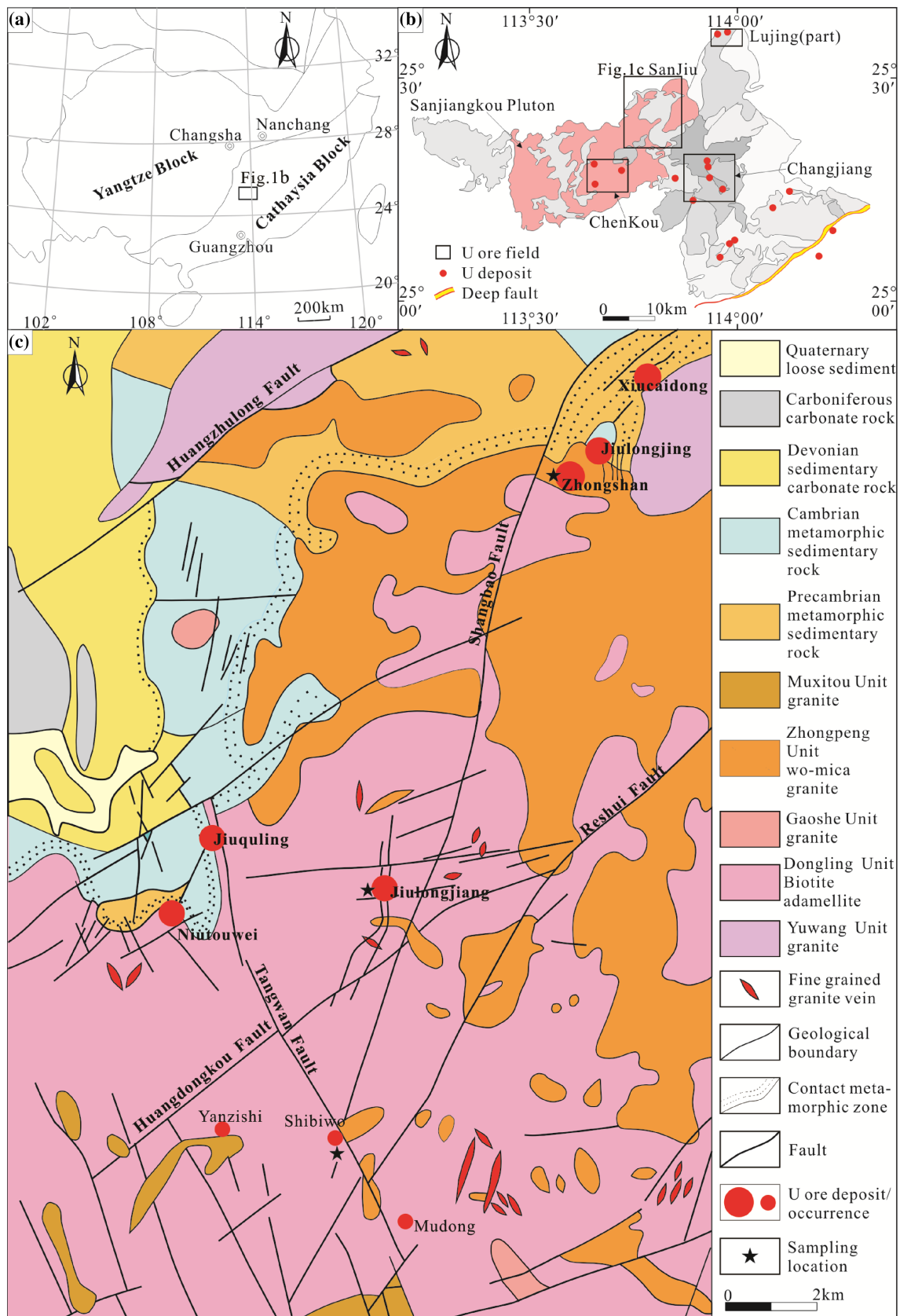
## 2 Geological settings

### 2.1 Regional geology

The SUOF is located within the center ZGB, an important part of Wanyangshan-Zhuguangshan strike-slip magmatic belt in the center of the Cathaysian Block (Zou et al. 2017), mainly composed of Triassic granites (nearly 934 km<sup>2</sup> outcrop area) and Jurassic granites (more than 2000 km<sup>2</sup> outcrop area). Several U ore fields (Lujing, Chengkou, Changjiang, etc.), many U deposits and U occurrences were discovered in the ZGB with high uranium content (9.0–19.6 ppm). The Sanjiangkou and Jiufeng granitic plutons constitute the EW-trending magmatic belt in the central ZGB (Fig. 1, Du et al. 2012; Chen et al. 2013).

### 2.2 Geology of the SUOF

The SUOF is named after the granite-related U deposits discovered in Jiulongjing, Jiuquling and Jiulongjiang ore districts and their surrounding areas (Fig. 1c). The exposed strata in the ore field are the Precambrian and Cambrian both composed principally of U-rich metamorphic sedimentary rocks, the Devonian composed of clastic sedimentary rocks and neritic carbonate rocks, the Carboniferous composed principally of neritic carbonate rocks, and the Quaternary composed of loose sediments. Jurassic granites cover most of the SUOF, which can be divided into two big granitic plutons (Fig. 1c): (1) the Sanjiangkou medium to coarse-grained biotite adamellite, the principal ore-hosting granite of the deposits, (2) the Zhongpeng fine-grained two-mica granite, and some other granites and fine granite dikes emplaced in the Late Jurassic. Previous studies have shown that the Sanjiangkou pluton belongs to highly fractionated peraluminous-strongly peraluminous S-type granite with the emplacement age of  $161.9 \pm 2.1$  Ma (Lan et al. 2018), and the Zhongpeng pluton belongs to high-potassium calc-alkaline peraluminous S-type granite with the emplacement age of  $148.2 \pm 1.9$  Ma (Lan, 2015; Wang et al. 2017). Previous studies suggest that these Late Jurassic granites are mainly of crust origin and have great potential for uranium exploration (Fei et al. 2012; Lan, 2015; Wang et al. 2017; Lan et al. 2018). The Suichuan-Reshui Fault (known as Shangbao-Reshui Fault pass through the SUOF) is one of



the deep faults in the Mesozoic-Cenozoic NE strike-slip orogenic belt in South China. It extends from Xiangshan in Jiangxi Province to Chengkou in Guangdong Province, with a total length of more than 300 km and an average strike of NE 30°. The fault is mainly convergent strike-slip in Jurassic and transited to discrete strike-slip in Cretaceous (Li et al. 2000). The main ore-controlling faults in the SUOF are NE-NNE and NW-trending secondary faults, which are located within or near the Shangbao-Reshui deep fault (Fig. 1c).

### 2.3 Deposit geology

Granite-related U deposits in the SUOF are of medium–low temperature hydrothermal origin, which can be divided into two subtypes: endogranitic and perigranitic. Some ore districts have two subtypes of U deposits (e.g., Jiuquling and Zhongshan deposit), and some only one subtype (e.g., Jiulongjiang endogranitic deposit). Uranium orebodies occur mainly in the turning, expanding and branching parts of ore-controlling faults, and the fracture zones in the strata, most of which present as continuous veins and network veins. There are three main ore types in the SUOF, which are siliceous vein type (svt), breccia type (bt) and altered cataclastic type (act). Uranium mineralization is usually closely related to the dark-red microcrystalline quartz-chalcedony vein, gray-white reticulated quartz, purple-black fluorite, granitic cemented breccia, and altered granitic cataclastic rock occur in ore-controlling faults (Du et al. 2012; Chen et al. 2013).

### 3 Sample descriptions

Hand specimens (ores) collected from boreholes in the SUOF are similar in lithology but differ greatly in grade (Figs. 1c, 2). According to the sample collection area, pyrite acquired from the ores is divided into three groups: Py X, Py J and Py S (Table 1). Based on the relationship between pyrite and uranium mineral, pyrites can be classified into two categories: Py I (U-related pyrite) and Py II (U-unrelated pyrite). Through the microscopic observation of pyrites, we found that Py I is generally anhedral colloform, veinlet and granular (particle size is generally 10–50  $\mu\text{m}$ , Fig. 2a–d, f, k), a little pyrite is fragmented and eroded internally, but whole assumes euhedral (particle size up to  $n \times 10 \mu\text{m}$ , Fig. 2g, h); Py II is euhedral-subhedral granular cube (particle size is generally 30–100  $\mu\text{m}$ , Fig. 2e, f, j).

The ore minerals are mainly pitchblende and uraninite. Coffinite, brannerite, are uranothorite and uncommon. Our unpublished studies show that pitchblende mainly occurs as micro-oolitic-grains and micro-veins with the age of

15–105 Ma. The gangue minerals include microcrystalline quartz, pyrite, hematite, fluorite, calcite, chlorite, and some clay minerals. Based on cross-cutting and replacement relationships, the paragenesis minerals in the SUOF can be divided into three stages and one period (Table 2).

## 4 Analytical methods

### 4.1 Major element analysis by EMPA

The mineralogical study was performed at the State key laboratory of nuclear resources and environment of the East China University of Technology using an optical microscope and using a Nova Nano-SEM 450 scanning electron microscope (SEM) and a JEOL JXA 8100 electron microprobe (EMPA). EMPA analytical conditions were 15 kV accelerating voltage, 50 nA beam current with a 1  $\mu\text{m}$  beam diameter for the major element analysis of pyrites. Detailed operating conditions for the SEM and the EMPA were described in Guo et al. (2012) and Wang et al. (2015).

### 4.2 In-situ Fe and trace element analysis by LA-ICP-MS

In-situ Fe and trace element analysis of pyrites was conducted by LA-ICP-MS at the Wuhan Sample Solution Analytical Technology Co., Ltd., China. Detailed operating conditions for the laser ablation system and the ICP-MS instrument and data reduction are the same as a description by Zong et al. (2017). Laser sampling was performed using a GeolasPro laser ablation system that consists of a COMPexPro 102 ArF excimer laser (wavelength of 193 nm and maximum energy of 200 mJ) and a MicroLas optical system. An Agilent 7700e ICP-MS instrument was used to acquire ion-signal intensities. Helium was applied as a carrier gas. Argon was used as the make-up gas and mixed with the carrier gas via a T-connector before entering the ICP. A “wire” signal smoothing device is included in this laser ablation system (Hu et al. 2015). The spot size and frequency of the laser were set to 32  $\mu\text{m}$  and 5 Hz, respectively, in this study. Trace element compositions of pyrites were calibrated against various reference materials (NIST 610 and NIST 612) without using an internal standard (Liu et al. 2008). The sulfide reference material of MASS-1 (USGS) was used as the unknown sample to verify the accuracy of the calibration method. Each analysis incorporated a background acquisition of approximately 20–30 s followed by 50–60 s of data acquisition from the sample. An Excel-based software ICPMSDataCal was used to perform off-line selection and integration of background and analyzed signals, time-drift

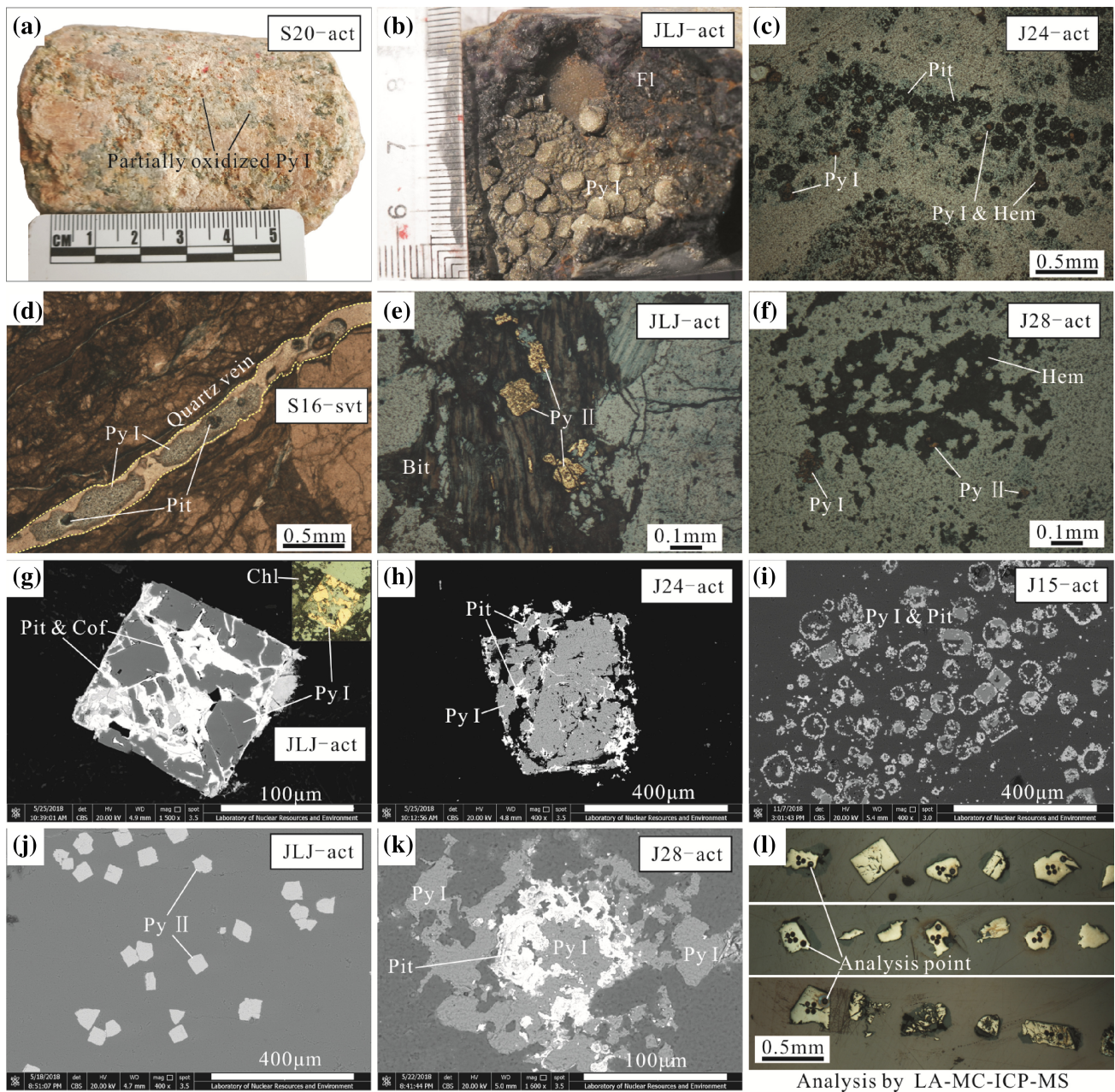


**Fig. 2** Photographs of pyrites from the SUOF. **a** altered Fractured granite with pyrite; **b** pyrite micro-particles and purple-black fluorite. **c** Colloidal pyrites, hematites and oolitic pitchblendes. **d** Colloidal pyrites and oolitic pitchblendes in quartz vein. **e** Euhedral and subhedral pyrites in biotite. **f** Colloidal pyrites, subhedral pyrites and disseminated hematites. **g** Fractured euhedral pyrite with microfractures filling in pitchblendes and coffinites. **h** Euhedral pyrite replaced by pitchblendes. **i** Pyrites replaced by pitchblendes and coffinites. **j** Euhedral pyrites and a small amount of pitchblendes. **k** Pitchblende occurs in dissolving anhedral pyrite. **l** Pyrites and part of laser in-situ analysis points. *Py* pyrite, *Hem* hematite, *Pit* pitchblende, *Cof* coffinite, *Fl* fluorite, *Qtz* quartz

correction and quantitative calibration for trace element analysis (Liu et al. 2008). The analytical precision of trace elements is evaluated to be better than 10%, and the detection limit generally varies from 0.0001 to 1 ppm.

### 4.3 In-situ S isotope analysis by LA-MC-ICP-MS

In-situ S isotope analysis of pyrites were performed on a Neptune Plus MC-ICP-MS equipped with a GeolasPro HD excimer ArF laser ablation system at the Wuhan Sample Solution Analytical Technology Co., Ltd., China. In the laser ablation system, helium was used as the carrier gas for the ablation cell and was mixed with argon (makeup



width from 5% to 95% of the full peak height) that was always greater than 5000.

A standard-sample bracketing method (SSB) was employed to correct for instrumental mass fractionation. To avoid the matrix effect, a pyrite standard PPP-1, was chosen as reference materials for correcting the natural pyrite samples. The reference value of  $\delta^{34}\text{S}_{\text{V-CDT}}$  in the standards has been reported by Fu et al. (2016). In addition, the in-house references of a pyrrhotite SP-Po-01 ( $\delta^{34}\text{S}_{\text{V-CDT}} = 1.4 \pm 0.4$ ) and a chalcopyrite SP-CP-01 ( $\delta^{34}\text{S}_{\text{V-CDT}} = 5.5 \pm 0.3$ ) were analyzing repeatedly as unknown samples to verify the accuracy of the calibration method. The uncertainty (Delta-2SE) of S isotope analysis generally ranges from 0.05 to 0.26. More detail of the in-situ S isotope ratios analysis was described in Fu et al. (2016).

#### 4.4 He and Ar isotopes analysis by Helix SFT

Pyrite samples were analyzed for He and Ar isotopic compositions using an all-metal extraction line coupled mass spectrometer (Helix SFT) at the Analytical Laboratory Beijing Research Institute of Uranium Geology, China National Nuclear Corporation (CNNC), China. The sensitivities of the Helix SFT for He were  $> 2 \times 10^{-4}$  A/Torr at 800  $\mu\text{A}$ , and for Ar  $> 7 \times 10^{-4}$  A/Torr at 200  $\mu\text{A}$ , respectively. The resolution of Faraday is more than 400, and the resolution of the multiplier is superior to 700 which can completely separate  $^3\text{He}$  and HD+. The system blank was measured according to the same procedure for the sample analysis but without crushing the sample, and He and Ar blanks were below  $2 \times 10^{-11}\text{cm}^3$  STP and  $1 \times 10^{-10}\text{cm}^3$  STP, respectively. Gas abundance was measured by peak–height comparison with known amounts of standard air from an air bottle with  $^3\text{He}/^4\text{He}$  ratio  $1.399 \times 10^{-6}$  and  $^{40}\text{Ar}/^{36}\text{Ar}$  ratio 295.5, and the size of the pipettes of He and Ar is 2516  $\text{cm}^3$  STP. More details of the He–Ar isotopes analysis were described in Li et al. (2015) and Xie et al. (2016).

## 5 Results

### 5.1 Major element

In this paper, EMPA was used to analyze the major elements of 22 spots in 6 pyrite samples from the SUOF, and Zou et al. (2017) analyzed the major elements of 31 spots in 5 pyrite samples from the SUOF and its adjacent area (Table 3). The results show that Fe contents of pyrites range from 42.14% to 47.81%, average 46.18%, and S contents of pyrite range from 43.77% to 53.69%, average 51.01%.

A total of 53 spots of 6 pyrites samples were analyzed for major elemental contents also by LA–ICP–MS. The results show that the contents of Fe range from 43.28% to 46.50%, average 45.89%, the contents of S range from 44.86% to 51.53%, average 50.19%. Pyrites show chemical compositions from  $\text{FeS}_{1.809}$  to  $\text{FeS}_{2.020}$ , with an average of 1.944 (Table 3). The theoretical chemical composition of pyrite is  $\text{FeS}_2$ , with the contents of Fe and S are 46.55% and 53.45%, respectively. It shows that pyrites in the SUOF and its adjacent area are generally deficient in S (Fig. 3). We concluded that pyrites in high-grade ore (Py J) are more deficient in S than those in low-grade ore (Py S and Py X).

### 5.2 Trace element

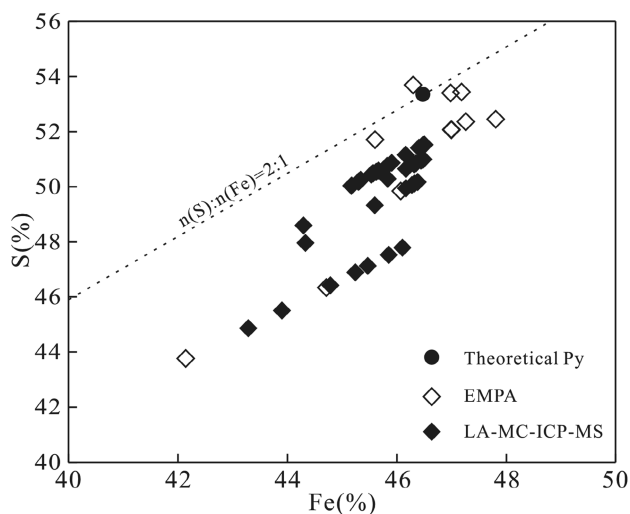
A total of 53 spots of 6 pyrites samples were analyzed for trace elemental contents. The contents of chalcophile elements (e.g., Cu, Pb, Zn, As, and Se) and siderophile elements (e.g., Co, Ni, Sn, and Ti) in pyrite are mostly above the detection limit. However, the contents of In, Cs, V, Ba, W, Au, Th and REE were below or near the detection limit. The contents of some trace elements vary widely, such as Si (221–13925 ppm), As (4–16783 ppm), Pb (0.01–3200 ppm), U (0–26715 ppm), etc. The high Si and U content of some samples or spots may be due to the heterogeneity of pyrites or the mixing of nano-sized sulfide particles (Ciobanu et al. 2012). Zou et al. (2017) suggested that pyrite rich in As is closely related to uranium minerals. As will enhance the chemical activity of S and make S easier to reduce U. This may be the reason why some samples have very high As and U content. Some samples or spots have a very high Pb content, mainly formed by decaying U. However, Some samples or spots have high U content but low Pb content, which may be due to Pb loss caused by later fluid.

### 5.3 Sulfur isotope

We analyzed 30 spots of 6 pyrites samples for  $\delta^{34}\text{S}$  isotope contents (analysis are normalized to Canyon diablo troilite V-CDT value), but the results of the sample X02 were obviously dispersed, possibly due to the diversity of sulfur sources (Table 4). The result shows that except for sample X02, the  $\delta^{34}\text{S}_{\text{V-CDT}}$  values of pyrites are a negative anomaly (vary from  $-14.86\%$  to  $-7.88\%$ , average  $-12.36\%$ ). According to the unpublished research data of No. 230 Uranium Geology Research Institute, the  $\delta^{34}\text{S}$  values of pyrites from the Zhongshan U deposit vary from  $-12\%$  to  $-5\%$ , which are similar to our analysis results.

**Table 3** EMPA major element contents (in wt%) of pyrites from the SUOF and its adjacent area

Sample	Number of tests	Fe	S	n(S)/n(Fe)	Collection area
X02	n = 4	47.26	52.36	1.93	Xiucaidong
J15	n = 3	46.07	49.84	1.88	Jiulongjiang
J24	n = 3	47.81	52.45	1.91	
J28	n = 4	44.71	46.34	1.81	
S16	n = 4	46.99	52.06	1.93	Shibiwo
S20	n = 4	46.99	52.08	1.93	
LYP35 <sup>a</sup>	n = 22	45.60	51.71	1.98	SW, Lujing
LYP04 <sup>a</sup>	n = 1	47.18	53.43	1.97	NE, Lujing
LYP46 <sup>a</sup>	n = 3	46.98	53.40	1.98	Xiucaidong
LYP59 <sup>a</sup>	n = 1	46.30	53.69	2.02	Jiulongjiang
LYP40 <sup>a</sup>	n = 4	42.14	43.77	1.81	Jiuquling

<sup>a</sup>From Zou et al. (2017)**Fig. 3** Plot of Fe versus S contents of pyrites from the SUOF

#### 5.4 Helium–Argon isotope

The He–Ar isotopes of fluid inclusions in 5 pyrites samples were analyzed (Table 5). The  $^3\text{He}/^4\text{He}$  ratios range from  $0.008 \pm 0.001$  to  $0.034 \pm 0.002$  (Ra represents the  $^3\text{He}/^4\text{He}$  ratio of air,  $1\text{Ra} = 1.40 \times 10^{-6}$ ), with an average ratio of 0.025. The concentrations of  $^3\text{He}$  range from  $11.76 \times 10^{-15}$  to  $17.70 \times 10^{-15} \text{cm}^3 \text{STP/g}$ , with an average of  $14.94 \times 10^{-15} \text{cm}^3 \text{STP/g}$ . The concentrations of  $^4\text{He}$  range from  $2.80 \times 10^{-7}$  to  $1.250 \times 10^{-6} \text{cm}^3 \text{STP/g}$ , with an average of  $5.42 \times 10^{-7} \text{cm}^3 \text{STP/g}$ . The concentrations of  $^{40}\text{Ar}$  range from  $4.31 \times 10^{-8}$  to  $8.11 \times 10^{-8} \text{cm}^3 \text{STP/g}$ , with an average of  $6.88 \times 10^{-8} \text{cm}^3 \text{STP/g}$ .  $^{40}\text{Ar}/^{36}\text{Ar}$  ratios are range from  $307.5 \pm 0.4$  to  $430.8 \pm 0.6$ , with an average ratio of 351.0, which is higher than the atmosphere  $^{40}\text{Ar}/^{36}\text{Ar}$  ratio (295.5).  $^{38}\text{Ar}/^{36}\text{Ar}$  ratios range from  $0.189 \pm 0.002$  to  $0.192 \pm 0.003$ , with an average of 0.191, which is close to the atmospheric ratio (0.188).

**Table 4** LA–MC–ICP–MS sulfur isotopic compositions (in ‰) of pyrites from the SUOF

Sample	Spot no.	$\delta^{34}\text{S}_{\text{V-CDT}}$	Sample	Spot no.	$\delta^{34}\text{S}_{\text{V-CDT}}$
X02	1	− 2.96	J28	1	− 13.15
	2	11.01		2	− 12.90
	3	0.48		3	− 13.36
	4	− 0.11		4	− 12.78
	5	5.38		5	− 14.30
	Average	2.76		Average	− 13.30
J15	1	− 14.08	S16	1	− 12.46
	2	− 13.63		2	− 12.25
	3	− 14.03		3	− 12.55
	4	− 14.47		4	− 11.52
	5	− 14.86		5	− 7.88
	Average	− 14.21		Average	− 11.33
J24	1	− 12.98	S20	1	− 8.65
	2	− 11.21		2	− 11.43
	3	− 13.11		3	− 10.85
	4	− 13.70		4	− 11.69
	5	− 13.29		5	− 12.92
	Average	− 12.86		Average	− 11.11

## 6 Discussion

### 6.1 Petrographic characteristics of pyrites and uranium mineralization

#### 6.1.1 Morphology of pyrites

As we referred to earlier, Py I has a generally irregular colloidal, vein-like and micron-sized granular texture (with larger relative surface area and easier to participate in geochemical reaction). Uranium does not enter the lattice

**Table 5** He–Ar isotopic compositions of fluid inclusions trapped in pyrite from the SUOF

Sample	$^{40}\text{Ar}/^{36}\text{Ar}$ ( $\pm 1\sigma$ )	$^{38}\text{Ar}/^{36}\text{Ar}$ ( $\pm 1\sigma$ )	$^{40}\text{Ar}$ ( $\text{cm}^3$ STP/g)	R/Ra ( $\pm 1\sigma$ )	$^3\text{He}$ ( $\text{cm}^3$ STP/g)	He ( $\approx$ $^4\text{He}$ ) ( $\text{cm}^3$ STP/g)
X02	$307.5 \pm 0.4$	$0.190 \pm 0.003$	$7.31 \times 10^{-8}$	$0.008 \pm 0.001$	$14.00 \times 10^{-15}$	$1250 \times 10^{-9}$
Z03	$430.8 \pm 0.6$	$0.192 \pm 0.003$	$4.31 \times 10^{-8}$	$0.030 \pm 0.002$	$11.76 \times 10^{-15}$	$280 \times 10^{-9}$
J28	$315.6 \pm 0.3$	$0.192 \pm 0.003$	$8.05 \times 10^{-8}$	$0.034 \pm 0.002$	$17.61 \times 10^{-15}$	$370 \times 10^{-9}$
S03	$320.2 \pm 0.4$	$0.189 \pm 0.002$	$8.11 \times 10^{-8}$	$0.026 \pm 0.002$	$13.61 \times 10^{-15}$	$374 \times 10^{-9}$
S16	$380.7 \pm 0.4$	$0.190 \pm 0.002$	$6.62 \times 10^{-8}$	$0.029 \pm 0.002$	$17.70 \times 10^{-15}$	$436 \times 10^{-9}$
Average	351.0	0.191	$6.88 \times 10^{-8}$	0.025	$14.94 \times 10^{-15}$	$542 \times 10^{-9}$

R is the  $^3\text{He}/^4\text{He}$  ratio measured of the sample and Ra is the  $^3\text{He}/^4\text{He}$  ratio of the standard atmosphere ( $1.4 \times 10^{-6}$ )

of pyrite. Usually, U-bearing minerals were adsorbed on the surface of pyrite or filled in micro-fissures or dissolution voids. Compared with Py I, euhedral and/or subhedral Py II is generally present as with larger particle size (smaller relative surface area) and fewer mineral micro-fissures. In summary, the texture of Py I changed more significantly than those of Py II. These mineralogical characteristics indicate that Py I directly participated in or influenced U mineralization in a more active metallogenic geological environment. It should be noted that the structural changes from Py I to Py II are transitional. Therefore, it is necessary to combine other characteristics of pyrite to find out whether it is an effective prospecting indicator.

### 6.1.2 Associated minerals

Hematite and pyrite are common mineral assemblages due to their chemical-genetic relationship. The mineral assemblage is usually closely related to U mineralization because hematite formed by oxidized pyrite adsorb uranium reduced by pyrite (Du et al. 2011). In this study, we found that mineral assemblage of Py I and anhedral hematite earthy is widely present in the ore. In addition, other associated minerals of Py I are generally different from those of Py II. For example, Py I is commonly associated with dark-red hematite, dark-green chlorite, purple-black fluorite, and variegated microcrystalline quartz veins (Fig. 2b–d, f), and Py II is often associated with light-colored altered clay minerals, green fluorite, and white or colorless medium-coarse-grained quartz (Fig. 2e, j). In a word, the color of Py I associated minerals is significantly different from that of Py II. Through these detailed mineralogical observations, we propose that the mineral assemblage of anhedral pyrite and dark-colored anhedral minerals may be considered as an effective prospecting indicator. However, further mineralogical studies are still needed to find out why these associated minerals generally have a dark tone.

## 6.2 Major element compositions of pyrite and uranium mineralization

The chemical reaction formula  $(1-x)\text{FeS}_2 + \text{UO}_2^{2+} + x\text{H}_2\text{O} \rightarrow (1-x)\text{Fe}^{2+} + 2(1-x)\text{S}^0 + \text{UO}_{2+x}(\text{s}) + 2x\text{H}^+$  of pyrite with active U indicates that  $\text{S}^{2-}$  reduces  $\text{U}^{4+}$  and makes the metallogenic environment acidic (Descostes et al. 2010). It is difficult to study the relationship between the changing pH value of the metallogenic environment and uranium mineralization. However, we assume that the sulfur deficit (as  $[2 - n(\text{S})/n(\text{Fe})]$ ) pyrite at the mineralization stage may indicate the potential of uranium mineralization.

## 6.3 Trace element compositions of pyrite and uranium mineralization

Trace elements can be hosted three ways in pyrite: (1) isomorphism; (2) micron-sized mineral inclusions; (3) nano-sized mineral particles. The distribution of trace elements in pyrite determines the shape of LA-ICP-MS analysis signals. The signals of trace elements in pyrite lattice (isomorphism) and uniformly distributed in nanoparticles are mainly smooth lines, and the signals of trace elements in inclusions are mainly characterized by large fluctuation curves (Leng 2017; Cook et al. 2016). Previous studies on pyrite in hydrothermal deposits have shown that As, Se, Co, Ni, Mn, and Mo either replace major elements or occur in homogeneous nanoparticles, while Ag, Cu, Zn, Sb, V, Ti, W, Pb, Th, and U usually occur in inclusions (Belousov et al. 2016; Leng 2017).

The trace element analysis signals of pyrite in this paper have various shapes consistent with previous studies. The signals of As, Se, Co, and Ni are basically flat in the middle of the profile, similar to that of Fe (Fig. 4a), indicating that they enter the pyrite lattice and displace the major elements (isomorphism). The signal of Si is always present and almost flat (Fig. 4b), indicating that it mainly occurs in a homogeneous nanoparticle. The signal of P is mainly relatively flat with a few fluctuations similar to some elements (Fig. 4b), indicating that it may occur in nanoparticle and

inclusion. Most of the analytical signals of Cu, Zn, Ti, W, Pb, Th, and U fluctuate greatly with a few similar fluctuations locally (Fig. 4b), indicating that they mainly occur in inclusions and a few in nanoparticles. The signals of REE elements and U have very similar fluctuations, indicating that they occur in the same inclusion (Fig. 4c). The trace elements (e.g., Si, P) that occur in nanoparticles are easily affected by metamorphic fluids. The ore grade and the average content of these elements occur in the pyrite lattices and inclusion (e.g., As, Se, Pb, Mo, REE) show a positive linear relationship approximately (Fig. 5), suggesting that these trace elements can be regarded as geochemical prospecting indicators, due to their migration and enrichment trend similar to U in ore-forming fluids.

The content or ratios of some trace elements (e.g., Co, Ni, and Th) in pyrite can be used to identify the pyrite genesis. The Co content of pyrite is positively correlated with the formation temperature of pyrite, while the Co and Ni contents of pyrites in our study are mostly low (mostly < 20 ppm, < 10 ppm, respectively), indicating that pyrites are mainly formed at low-temperature (Mei, 2000). The Co/Ni ratios of pyrites mostly vary from 1 to 10 (Fig. 6), indicating that pyrites are mainly magmatic-hydrothermal ( $1 < \text{Co/Ni} < 5$ ) or volcanic hydrothermal ( $\text{Co/Ni} > 5$ ) genesis (Xu and Shao 1980; Chen et al. 1987; Bajwah et al. 1987; Brill 1989; Zheng et al. 2006). The Th contents of pyrites are generally lower than the detection limit, which leads to a very low Th/U ratios, suggesting that pyrites are of hydrothermal origin (Liu et al. 2018). Therefore, we consider that the uranium mineralization is mainly of low-temperature hydrothermal genesis.

Due to similar geochemical properties, both of REE and U mainly occurs as uranium carbonate complexes and migrated in ore-forming fluids. Therefore, pitchblende in hydrothermal U deposits is generally rich in REE (McLennan and Taylor 1979; Weaver et al. 1987; Xiong and Zhai, 1991). Our analysis shows that the chondrite-

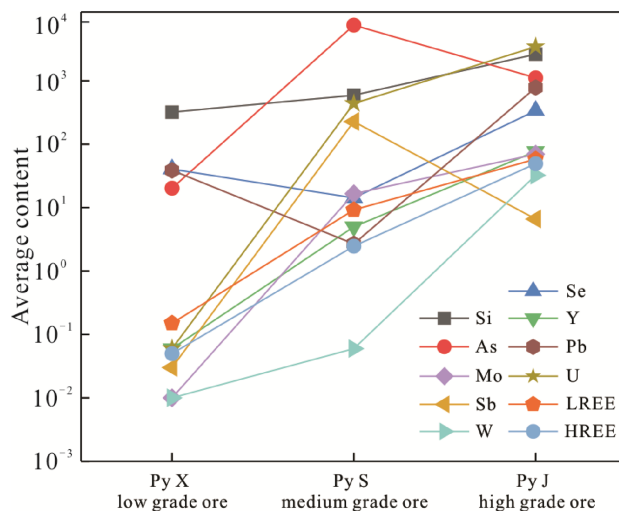


**Fig. 5** Plot of average content of trace elements of pyrites from different areas of the SUOF

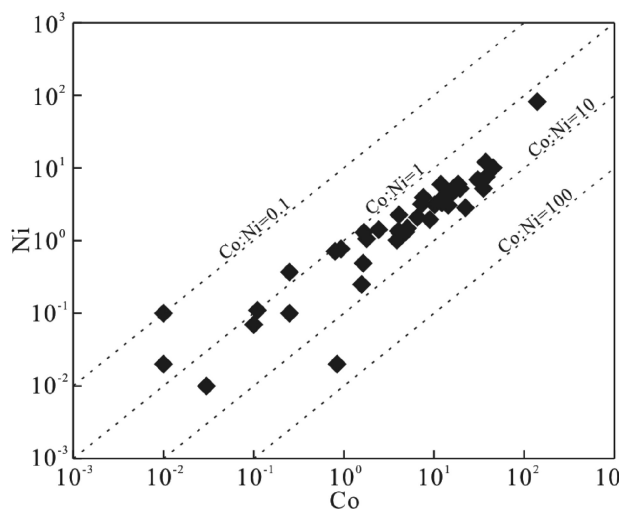


**Fig. 6** Plot of Co versus Ni contents of pyrites from the SUOF

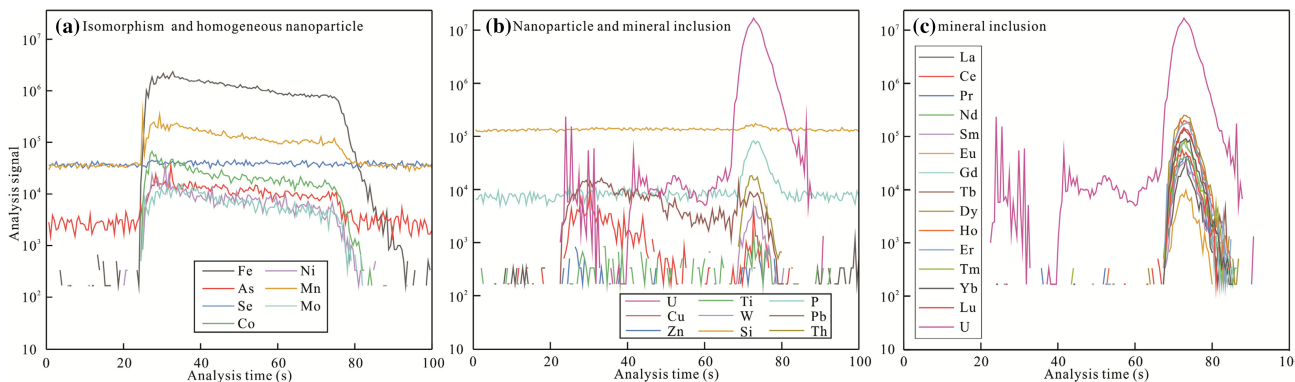


**Fig. 4** LA-ICP-MS analysis signal profile for selected elements of representative pyrite in ore from the SUOF

normalized REE patterns of pyrite inclusions are similar to those of Sanjiangkou pluton and pitchblende (Fig. 7), suggesting that the sources of pyrite and pitchblende may come from granitic pluton. The LREE distributions of pyrites in Shibiwo occurrence are quite different, probably due to the CO<sub>2</sub> content of ore-forming fluid changes rapidly, and the stability of LREE complex is far inferior to that of HREE complex (Huang et al. 2010). In addition, we found that pyrite  $\sum$ REE is positively correlated with ore grade. The higher the ore grade, the closer the chondrite-normalized REE patterns of pyrite inclusion is to that of granitic pluton (Fig. 7), suggesting that pyrite with high REE content may be a useful prospecting indicator.

### 6.4 Isotopic compositions of pyrites and ore-forming fluids

#### 6.4.1 Sulfur isotopic compositions of pyrites

Seal (2006) pointed out that the oxidation–reduction process will change the content of <sup>34</sup>S in sulfide. Our test results show that the δ<sup>34</sup>S values of samples (except X02) are mainly negative (vary from − 14.86‰ to − 7.88‰), indicating that the ore-forming fluid is in a relatively stable reduction environment, promoting the reduction and precipitation of uranium minerals. The δ<sup>34</sup>S isotopic composition of pyrite from the SUOF (central part of

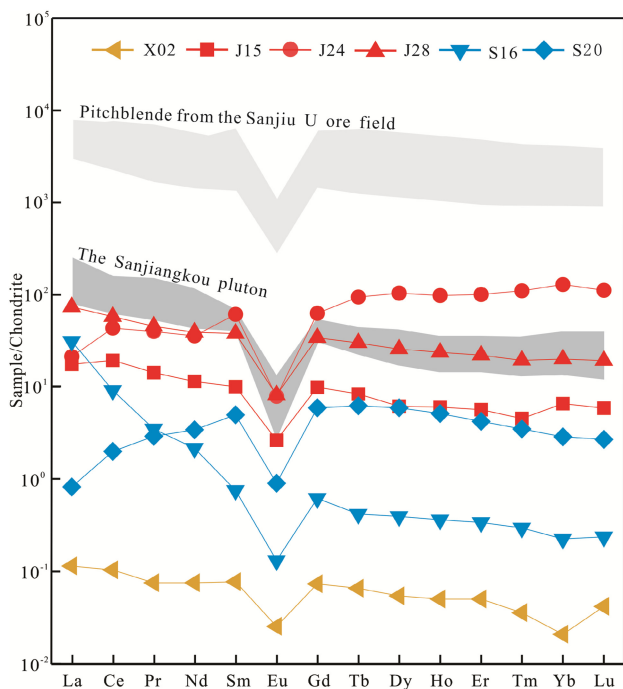


**Fig. 7** Chondrite-normalized REE patterns of pyrites inclusions from the SUOF. The normalized values are based on Sun and McDonough (1989); The Sanjiangkou Pluton (Lan et al. 2018); Pitchblende (Our unpublished data)

Zhuguangshan) and some U deposits/occurrence in southern part of Zhuguangshan is mainly in the distribution range among sedimentary sulfur, metamorphic sulfur, biogenesis sulfur, and maybe partly derived from granite (X02, vary from − 2.96‰ to 11.01‰), obviously different from that of the mantle and the deposits in Lujing ore field (Fig. 8). The <sup>34</sup>S isotopic compositions of pyrites from the SUOF indicate that the ore-forming fluids may be poor in <sup>34</sup>S and rich in <sup>32</sup>S. In addition, we found that pyrite <sup>34</sup>S<sub>v-CDT</sub> value is negatively correlated with ore grade (Fig. 9). The lower content of pyrite <sup>34</sup>S, the higher ore grade (ore grade: Py X < Py S < Py J), suggesting that the richer U in ore-forming fluid, the lower <sup>34</sup>S.

#### 6.4.2 Helium–Argon isotopic compositions of pyrites

There may be three potential sources of He and Ar isotopes trapped in hydrothermal fluids, air-saturated water (ASW), the crust and the mantle, respectively (Simmons et al. 1987; Stuart et al. 1995; Burnard et al. 1999). The ASW, including meteoric water and seawater, which has a typical He and Ar isotopic composition of <sup>3</sup>He/<sup>4</sup>He = Ra, <sup>40</sup>Ar/<sup>36</sup>Ar = 295.5, and <sup>40</sup>Ar/<sup>4</sup>He ≈ 0.01. The crust-derived fluids have a He and Ar isotopic composition of <sup>3</sup>He/<sup>4</sup>He ≤ 0.1 Ra (mostly, vary from 0.01 Ra to 0.05 Ra), <sup>40</sup>Ar/<sup>36</sup>Ar ≥ 45,000, and <sup>40</sup>Ar/<sup>4</sup>He ratios vary from 0.16 to 0.25. The mantle-derived fluids have a He and Ar isotopic composition of <sup>3</sup>He/<sup>4</sup>He ratios vary from 6 Ra to 9 Ra, <sup>40</sup>Ar/<sup>36</sup>Ar > 40,000, and <sup>40</sup>Ar/<sup>4</sup>He ratios vary from 0.33 to 0.56 (Burnard et al. 1999). The content of He in the earth’s atmosphere is quite low and the solubility of He in low-temperature aqueous solution is very low. Therefore, ASW

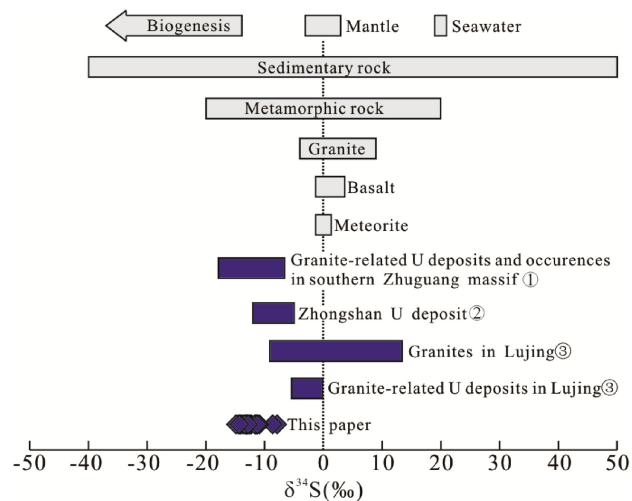


**Fig. 8** S isotope distribution of pyrites from the SUOF. Base map after Zhang et al. (2012) and Lu et al. (2015); (1) from Lu et al. (2015); (2) from No. 230 institute, CNNC; (3) from Wang et al. (1999)

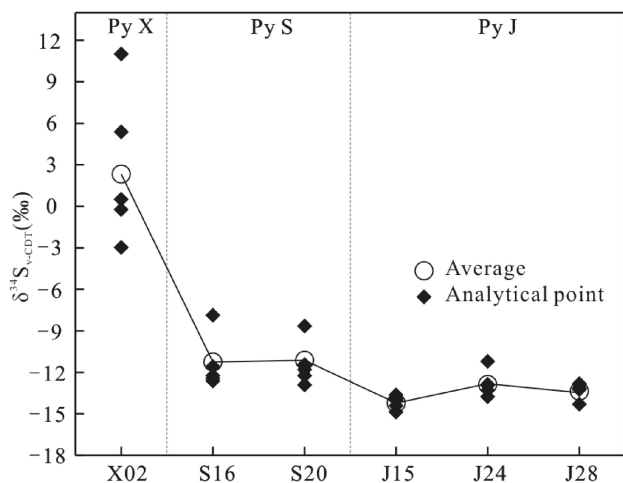


**Fig. 9** Plot of  $\delta^{34}\text{S}_{\text{V-CDT}}$  contents of pyrites from the SUOF

has little effect on the abundance and composition of He isotopes of most crustal and mantle fluids (Stuart et al. 1995; Burnard et al. 1999). It is considered that the He of ore-forming fluids in the SUOF may come from the crust and/or mantle.

The  $^3\text{He}/^4\text{He}$  ratios of fluid inclusions trapped in pyrites from the SUOF vary from 0.008 Ra to 0.034 Ra, close to crustal values ranging from 0.01 to 0.05 Ra (Stuart et al. 1995). The  $^3\text{He}$ - $^4\text{He}$  isotopic compositions of pyrite fluid inclusions are in or very close to the crustal He isotopic values (Fig. 10a) and the He–Ar isotopic compositions are in or very close to the crustal fluid (Fig. 10b), both of which indicate that the ore-forming fluids are basically derived from the crust and are not or seldom affected by the mantle fluids. If the ore-forming fluids are a simply mixed origin of mantle fluid and crustal fluid, the ratio of pyrite  $^3\text{He}/^4\text{He}$  is the weighted average value of those of mantle fluid and crustal fluid, and the ratio of the two fluids in ore-forming fluids can be calculated (Stuart et al. 1995; Xu 1996). The formula is  $^4\text{He}_m (\%) = [(R_s - R_c)/(R_m - R_c)] \times 100$ , where  $R_s$  is  $^3\text{He}/^4\text{He}$  ratio of pyrite,  $R_c$  is  $^3\text{He}/^4\text{He}$  ratio of the crust and  $R_m$  is  $^3\text{He}/^4\text{He}$  ratio of the mantle ( $R_c = 0.01$ – $0.05$  Ra,  $R_m = 6$ – $9$  Ra, Stuart et al. 1995). The calculation results show that the proportion of mantle fluids in ore-forming fluids is about 0.18%–0.40%. Previous studies have shown that the Jurassic granites in the Sanjiu area were formed by partial melting of lower crustal strata, with a small amount of mantle material (Fei et al. 2013; Zhang et al. 2014a, b; Lan et al. 2018). Therefore, the ore-forming fluids in the SUOF are mainly crustal fluids, which may be mixed with a very small amount of mantle fluids.

It should be pointed out that our conclusions seem to be different from previous research. According to the composition of noble gases (Fig. 10a, Zhang et al. 2010), the ore-forming fluids of the No. 302 U deposit in the

Changjiang U ore field were characterized by crust-mantle mixing, and the proportion of mantle-derived components in the ore-forming fluids are significantly higher than that in the SUOF. The exploration depth of SUOF (mostly < 500 m) is much shallower than that of the Changjiang orefield (> 1000 m). Chen et al. (2019a) showed that the average emplacement depth of granitic plutons in the Changjiang U ore field (about 18 km) is obviously deeper than that of the SUOF (about 13 km). There are many hot springs in these U ore fields, which indicate that these plutons are high heat production (HHP) granites and can promote the deep thermal cycle of ore-forming fluids (Cuney 2014). The emplacement depth and ore-forming elevation of U-bearing pluton determine the geothermal and pressure of ore-forming fluids, which may be the reason for the difference in the properties of ore-forming fluids (the proportion of mantle-derived fluids). We speculate that the metallogenic models of U deposits may be quite different even in the same granitic batholith, but more work is needed to test this hypothesis.

## 6.5 Pyrite and metallogenic model

After the extraction of uranium from Mesozoic granites, multi-source fluids formed ore-forming fluids. A large number of  $\text{U}^{6+}$  in ore-forming fluids interacted with various reductants such as S in pyrite gradually precipitated and formed uranium minerals rich in  $\text{U}^{4+}$ , and finally formed uranium deposits.

### 6.5.1 Formation of ore-forming fluids

During the Mesozoic (Late Cretaceous to the Tertiary), the tectonic regime of South China changed to large-scale extension (Hu et al. 2008), and the oxidized surface-derived fluids, mainly meteoric water origin, infiltrated along regional strike-slip faults, the contact zone of granites, secondary faults and brittle-tensional fissures from shallow to deep. A great number of surface-derived fluids mixed with a few metamorphic fluids of granites and sedimentary rocks to form crustal-derived fluids. The Triassic and Jurassic period U-rich granites were subjected to alteration, and U in accessory minerals (e.g., uraninite and monazite) was liberated into the vicinity and/or partitioned into crustal-derived fluids (Hu et al. 2012; Bonnetti et al. 2018). The crustal-derived fluids also extracted many elements, such as Fe and S, from U-rich geological bodies (mainly U-rich granites and strata) and mixed with a high-temperature mantle-derived fluids during deep fluid circulation. In the upwelling process, these mixed fluids were remixed with new crustal-derived fluids, which made the proportion of mantle-derived fluids decrease gradually. These new mixed fluids eventually surged along tensional

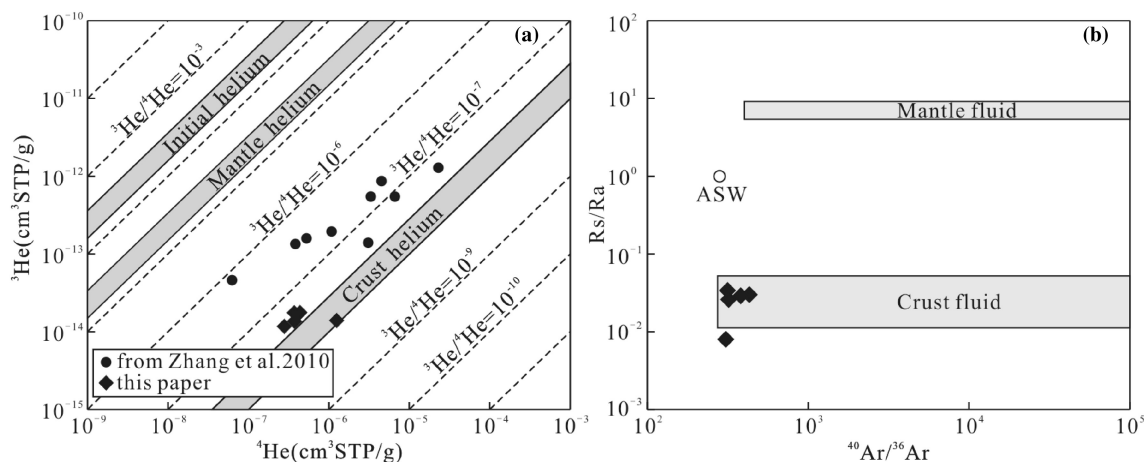
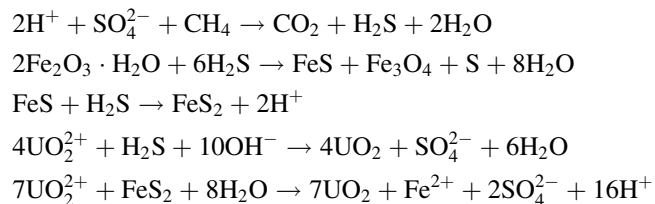


**Fig. 10** **a** Plots of  ${}^3\text{He}$  versus  ${}^4\text{He}$  (after Mamyryn and Tolstikhin 1984); **b**  $R_s/R_a$  versus  ${}^{40}\text{Ar}/{}^{36}\text{Ar}$  (after Hu et al. 2009) of the fluids trapped in pyrites from the SUOF

faults and became medium–low temperature ore-forming fluids.

### 6.5.2 The promotion of pyrite to mineralization

Uranium occurs predominantly in a hexavalent state ( $\text{U}^{6+}$ ) as uranyl carbonate complexes and uranyl fluorides in the ore-forming fluids; Fe and S occur mainly as  $\text{Fe}^{2+}$ ,  $\text{H}_2\text{S}$ ,  $\text{S}_2\text{O}_3^{2-}$ ,  $\text{S}_4\text{O}_6^{2-}$ ,  $\text{SO}_3^{2-}$  and  $\text{SO}_4^{2-}$  (Cuney 1978; Descostes et al. 2010). The ore-controlling interfaces, such as near-surface ore-controlling faults, pluton contact zones, and interlayer fracture zones, are relatively reducing metallogenic environments characterized as medium–low temperature, low pressure and acidity. Uranyl carbonate complexes destabilized, releasing  $\text{U}^{6+}$  when the ore-forming fluid upwelled and flowed through the ore-controlling interfaces. Under complex metallogenic geological conditions (T, pH,  $f(\text{O}_2)$ ),  $\text{U}^{6+}$  was reduced to  $\text{U}^{4+}$  by  $\text{S}^{2-}$ ,  $\text{HS}^-$ ,  $\text{Fe}^{2+}$ ,  $\text{CH}_4$ ,  $\text{H}_2$ , etc., and finally formed uranium minerals such as pitchblende (Langmuir 1978; Wang and Du 1995; Liger et al. 1999; Chen et al. 2019a, b),  $\text{S}^{2-}$  was oxidized to  $\text{S}^0$ ,  $[\text{S}]_2^{2-}$  (Hu et al. 2004a, b; Descostes et al. 2010),  $\text{S}^{x+}$  may be reduced to  $\text{S}^0$ , saturated  $\text{Fe}^{2+}$  and  $[\text{S}]_2^{2-}$  formed pyrite. There may be some important chemical reactions of sulfide and uranium reduction can expressed as follows (Fontboté et al. 2017; Chen et al. 2019b):



At the mineralization stage, pitchblende and pyrite precipitate alternately (Cuney 1978). After precipitation

and enrichment of a large number of uranium minerals, U ore bodies or U deposits eventually formed at various ore-controlling interfaces.

## 7 Conclusions

1. U-related pyrites generally have poor crystal form, such as euhedral-subhedral with dissolution textures, anhedral variety with colloform texture, veinlet and fine particles, etc. The color of the associated minerals of U-related pyrite is generally significant dark hues, such as purple-black fluorite, dark-red hematite, dark-green chlorite, etc.
2. Pyrites are characterized by general S deficiency ( $\text{FeS}_{1.944}$ ), low content of Co and Th, and  $\text{Co}/\text{Ni} > 1$ , indicating that both pyrites and uranium deposits are of low-temperature hydrothermal origin. The trace elements (such as As, Se, REE) mainly exist in pyrite lattice or inclusions, which are consistent with the enrichment trend of U. They can effectively indicate granite-related U mineralization in the SUOF.
3. The higher the grade of ore, the more deficient S, and the higher  $\sum\text{REE}$  content of pyrite. These geochemical characteristics show that sulfur in pyrite, as an important reducing agent, participates in the reduction process of  $\text{U}^{6+}$ , the mineralization is in a relative reducing environment, and the REE can be regarded as an efficient prospecting indicator because of its similar migration and enrichment trend with uranium.
4. The S–He–Ar isotopic compositions of pyrites indicate that the ore-forming fluids mainly consist of complex crustal-derived fluids mixed with a small amount of mantle fluids. The complex crust-derived fluids are

mainly composed of surface-derived fluids of meteoric water origin, metamorphic fluids of granite and/or sedimentary rocks.

**Acknowledgements** This research was supported by the Science and Technology Research Project of China Nuclear Geology (No. 2110400024), Uranium Geological Exploration Fund Project of China National Nuclear Corporation (No. J2012-03), Uranium Mine Exploration Project of Hunan Nuclear Geology (No. DK306-20170512), Scientific Research Program of Hunan Nuclear Geology (No. KYQ-306-01). We are very grateful to Dr. Bin Wu of East China University of Technology for his assistance in EMPA analysis, Dr. Le Zhu of Wuhan Sample Solution Analytical Technology Co., Ltd for his help in LA-ICP-MS analysis, He-Ar isotopes analysis by Analytical Laboratory of Beijing Research Institute of Uranium Geology.

#### Compliance with ethical standards

**Conflict of interest** The authors declare that there is no conflict of interest.

## References

- Agangi A, Hofmann A, Przybyłowicz W (2014) Trace element zoning of sulfides and quartz at Sheba and Fairview gold mines: clues to Mesoproterozoic mineralisation in the Barberton Greenstone Belt, South Africa. *Ore Geol Rev* 56:94–114
- Bajwah ZU, Seccombe PK, Offler R (1987) Trace element distribution Co:Ni ratios and genesis of the Big Cadia iron–copper deposit, New South Wales, Australia. *Miner Dep* 22(4):292–300
- Belousov I, Large RR, Meffre S, Danyushevsky LV, Steadman J, Beardmore T (2016) Pyrite compositions from VHMS and orogenic Au deposits in the Yilgarn Craton, Western Australia: implications for gold and copper exploration. *Ore Geol Rev* 79:474–499
- Bonnetti C, Liu XD, Mercadier J, Cuney M, Deloule E, Villeneuve J, Liu WQ (2018) The genesis of granite-related hydrothermal uranium deposits in the Xiaozhuang and Zhuguang ore fields, North Guangdong Province, SE China: insights from mineralogical, trace elements and U–Pb isotopes signatures of the U mineralisation. *Ore Geol Rev* 92:588–612
- Brill BA (1989) Trace-element contents and partitioning of elements in ore minerals from the CSA Cu–Pb–Zn deposit, Australia, and implications for ore genesis. *Canad Miner* 27:263–274
- Burnard PG, Hu RZ, Turner G, Bi XW (1999) Mantle, crustal and atmospheric noble gases in Ailaoshan gold deposit, Yunnan Province, China. *Geochim Cosmochim Acta* 63:1595–1604
- Cai YQ, Zhang JD, Li ZY, Guo QY, Song JY, Fan HH, Liu WS, Qi FC, Zhang ML (2015) Outline of uranium resources characteristics and metallogenic regularity in China. *Acta Geol Sin* 89(6):1051–1106 (in Chinese with English abstract)
- Chen X, Zhang SF (2016) Study on the geological characteristics of uranium metallogenesis and the spatial distribution of uranium ore bodies in Jiulongjiang mining area in Sanjia area. *Land Resour Herald* 13:9–13 (in Chinese with English abstract)
- Chen GY, Sun DS, Yin HA (1987) Genetic and prospecting mineralogy. Chongqing Publishing House, Chongqing, pp 1–818 (in Chinese with English abstract)
- Chen X, Jiang BG, He YY, Sun LQ (2013) Geological survey report of Sanjiangkou Uranium Deposit, Rucheng, Hunan. The 306 team of Hunan Nuclear Geology, Hengyang (in Chinese)
- Chen X, Liu XD, Qin JN, Pan JY, Jiang BG (2019a) Geochemistry of biotite from the Sanjiangkou pluton in the Zhuguangshan massif terrane and its geological significance. *Bull Miner Petr Geochim* 38(05):1031–1040 (in Chinese with English abstract)
- Chen Y, Jin RS, Miao P, Li JG, Guo H, Chen LL (2019b) Occurrence of pyrites in sandstone-type uranium deposits: relationships with uranium mineralization in the North Ordos Basin, China. *Ore Geol Rev* 109:426–447
- Ciobanu CL, Cook NJ, Utsunomiya S, Kogagwa M, Green L, Gilbert S, Wade B (2012) Gold-telluride nanoparticles revealed in arsenic-free pyrite. *Am Miner* 97:1515–1518
- Cook NJ, Ciobanu CL, Mao JW (2009) Textural control on gold distribution in As-free pyrite from the Dongping, Huangtuliang and Hougou gold deposits, North China Craton (Hebei Province, China). *Chem Geol* 264:101–121
- Cook NJ, Ciobanu CL, George L, Zhu ZY, Wade B, Ehrig K (2016) Trace element analysis of minerals in magmatic-hydrothermal ores by laser ablation inductively-coupled plasma mass spectrometry: approaches and opportunities. *Minerals* 6(4):111
- Cuney M (1978) Geologic environment, mineralogy, and fluid inclusions of the Bois Noirs–Limouzat uranium vein, Forez, France. *Econ Geol* 73(8):1567–1610
- Cuney M (2014) Felsic magmatism and uranium deposits. *Bull Soc Géol Fr* 185(2):75–92
- Dehnavi AS, McFarlane CRM, Lentz DR, Walker JA (2018) Assessment of pyrite composition by LA-ICP-MS techniques from massive sulfide deposits of the Bathurst Mining Camp, Canada: from textural and chemical evolution to its application as a vectoring tool for the exploration of VMS deposits. *Ore Geol Rev* 92:656–671
- Deng P, Shu LS, Tan ZZ (2003) The geological setting for the formation of rich uranium ores in Zhuguang–Guidong large-scale uranium metallogenetic area. *Geol Rev* 49:486–494 (in Chinese with English abstract)
- Deng P, Ren JS, Ling HF, Shen WZ, Sun LQ, Zhu N, Tan ZZ (2012) SHRIMP zircon U–Pb ages and tectonic implications for Indosinian granitoids of southern Zhuguangshan granitic composite, South China. *Chin Sci Bull* 57:1231–1241 (in Chinese)
- Descostes M, Schlegel ML, Eglizaud N, Descamps F, Miserque F, Simoni E (2010) Uptake of uranium and trace elements in pyrite (FeS<sub>2</sub>) suspensions. *Geochim Cosmochim Acta* 74:1551–1562
- Du LT, Wang WG, Liu ZY (2011) Granite-related uranium deposits of research and evaluation of uranium deposits in China. China Nuclear Geology and Beijing Research Institute of Uranium Geology, Beijing (in Chinese)
- Du GS, Xiao ZH, Wang XJ, Li CH (2012) Study on uranium metallogenetic geological conditions and prospecting prospects in Sanjia area. The 302 team of Hunan Nuclear Geology, Chenzhou (in Chinese)
- Fan HH, Ling HF, Wang DZ, Shen WZ, Liu CS, Jiang YH (2001) Ore-forming material sources for Xiangshan uranium ore-field in Jiangxi Province: evidence from Nd–Sr–Pb isotopes. *Geol J Chin Univ* 7:139–145 (in Chinese with English abstract)
- Fei TW, Liu X, Qian JN, Xia ZQ, Jiang BG, Mei SQ (2012) Geological characteristics and genesis of uranium in Sanjiangkou orefield, Rucheng City, Hunan Province. *J Univ S Chin Sci Technol* 26(03):39–46 (in Chinese with English abstract)
- Fei TW, Luo Y, Sun X (2013) Ore-forming fluid features and metallogenetic model of uranium deposits in Zhuguangshan ore field. *World Nucl Geosci* 30:63–69 (in Chinese with English abstract)
- Fontboté L, Kouzmanov K, Chiaradia M, Pokrovski GS (2017) Sulfide minerals in hydrothermal deposits. *Elements* 13(2):97–103

- Fu JL, Hu ZC, Zhang W, Yang L, Liu YS, Li M, Zong KQ, Gao S, Hu SH (2016) In situ sulfur isotopes ( $\delta^{34}\text{S}$  and  $\delta^{33}\text{S}$ ) analyses in sulfides and elemental sulfur using high sensitivity cones combined with the addition of nitrogen by Laser Ablation MC–ICP–MS. *Anal Chim Acta* 911:14–26
- Fuchs S, Williams-Jones AE, Przybylowicz WJ (2016) The origin of the gold and uranium ores of the Black Reef Formation, Transvaal Supergroup, South Africa. *Ore Geol Rev* 72:149–164
- Guo GL, Zhang ZS, Liu XD, Feng ZS, Lai DR, Zhou WT (2012) EPMA chemical U–Th–Pb dating of uraninite in Guangshigou uranium deposit. *J E Chin Inst Technol Nat Sci Ed* 35:309–314 **(in Chinese with English abstract)**
- Hu RZ, Bi XW, Turner G, Burnard PG (1997) He–Ar isotopic systems of pyrite fluid inclusions in the Machangqing copper deposit. *Chin Sci Ser D* 27:503–508 **(in Chinese)**
- Hu RZ, Bi XW, Su WC, Peng JT, Li CY (2004a) The relationship between uranium metallogenesis and crustal extension during the Cretaceous-Tertiary in South China. *Earth Sci Front* 11(1):153–160 **(in Chinese with English abstract)**
- Hu SX, Ye Y, Fang CQ (2004b) Petrology of the metasomatically altered rocks and its significance in prospecting. Geological Publishing House, Beijing, pp 78–81 **(in Chinese with English abstract)**
- Hu RZ, Bi XW, Zhou MF, Peng JT, Su WC, Liu S, Qi HW (2008) Uranium metallogenesis in South China and its relationship to crustal extension during the Cretaceous to Tertiary. *Econ Geol* 103:583–598
- Hu RZ, Burnard PG, Bi XW, Zhou MF, Peng JT, Su WC, Zhao JH (2009) Mantle-derived gaseous components in ore-forming fluids of the Xiangshan uranium deposit, Jiangxi province, China: evidence from He, Ar and C isotopes. *Chem Geol* 266:86–95
- Hu H, Wang RC, Chen WF, Ding HH, Chen PR, Ling HF (2012) Study on uranium resource minerals of Douzhashan uranium-bearing granite, Northeastern Guangxi. *Geol Rev* 58:1056–1068 **(in Chinese with English abstract)**
- Hu ZC, Zhang W, Liu YS, Gao S, Li M, Zong KQ, Chen HH, Hu SH (2015) “Wave” signal-smoothing and mercury-removing device for laser ablation quadrupole and multiple collector ICPMS analysis: application to lead isotope analysis. *Anal Chem* 87:1152–1157
- Huang HL (2000) The senses of pyrite in discerning blind ores of uranium deposits. *Geol Min Resour Res* 15(1):72–76 **(in Chinese with English abstract)**
- Huang HY, Huang SD, Cai SF (2008) Analysis on geological setting of uranium mineralization and prospecting strategy in Lujing area, Hunan Province. *World Nucl Geosci* 25:63–67 **(in Chinese with English abstract)**
- Huang GL, Yin ZP, Ling HF, Deng P, Zhu B, Shen WZ (2010) Formation age, geochemical characteristics and genesis of pitchblende from No.302 uranium deposit in northern Guangdong. *Min Dep* 29:352–360 **(in Chinese with English abstract)**
- IAEA (2016) Geological classification of uranium deposits with description of selected examples. IAEA, Vienna
- Jiang BG, He YY, Chen X, Luo WQ, Tan Q, Qin JL (2017) Mineralization and metallogenic model of Sanjiangkou uranium deposit in San-jiu area. *Uranium Geol* 33(05):266–272 **(in Chinese with English abstract)**
- Khishgee C, Akasaka M, Ohira H, Sreenen J (2014) Gold mineralization of the Gatsuert deposit in the north Khentei gold belt, central northern Mongolia. *Resour Geol* 64:1–16
- Lan HF (2015) Geochronology, geochemistry, petrogenesis and uranium mineralization potential of Sanjiu area granites in southern Zhuguangshan composite pluton. Master’s thesis, Nanjing University, Nanjing, China **(in Chinese with English abstract)**
- Lan HF, Ling HF, Chen WF, Liu JW, Ouyang PN (2018) Study on petrogenesis and uranium mineralization potential of eastern Sanjiangkou granitic pluton. *Geol J Chin Univ* 24:172–185 **(in Chinese with English abstract)**
- Langmuir D (1978) Uranium solution-mineral equilibria at low temperatures with applications to sedimentary ore deposits. *Geochim Cosmochim Acta* 42(6):547–569
- Large RR, Danyushevsky L, Hollit C, Maslennikov V, Meffre S, Gilbert S, Bull S, Scott R, Emsbo P, Thomas H, Singh B, Foster J (2009) Gold and trace element zonation in pyrite using a laser imaging technique: Implications for the timing of gold in orogenic and Carlin-style sediment-hosted deposits. *Econ Geol* 104(5):635–668
- Leng CB (2017) Genesis of Hongshan Cu polymetallic large deposit in the Zhongdian area, NW Yunnan: constraints from LA–ICP–MS trace elements of pyrite and pyrrhotite. *Earth Sci Front* 24(6):162–175 **(in Chinese with English abstract)**
- Li JW, Li ZJ, Fu ZR, Li XF (2000) Heat sources and hydrothermal uranium mineralization in the Suichuan–Reshui strike-slip fault zone. *Geol Sci Technol Inf* 19(3):39–43 **(in Chinese with English abstract)**
- Li JJ, Li J, Liu HB, Zhang J, Jin GS, Zhang JF, Han J (2015) Helium isotopic composition of inclusions in mineral grains using Helix SFT noble gas mass spectrometer. *Acta Geol Sin* 89:826–1831 **(in Chinese with English abstract)**
- Liger E, Charlet L, Van Cappellen P (1999) Surface catalysis of uranium(VI) reduction by iron(II). *Geochim Cosmochim Acta* 63(19–20):2939–2955
- Liu YS, Hu ZC, Gao S, Günther D, Xu J, Gao CG, Chen HH (2008) In situ analysis of major and trace elements of anhydrous minerals by LA–ICP–MS without applying an internal standard. *Chem Geol* 257:34–43
- Liu GQ, Zhao KD, Jiang SY, Chen W (2018) In-situ sulfur isotope and trace element analysis of pyrite from the Xiwang uranium ore deposit in South China: implication for ore genesis. *J Geochem Expl* 195:49–65
- Lu HZ, Zhu XQ, Shan Q, Wang ZG (2013) Hydrothermal evolution of gold-bearing pyrite and arsenopyrite from different types of gold deposits. *Min Dep* 32:823–842 **(in Chinese with English abstract)**
- Lu XL, Zhu MQ, Wu T (2015) Study on the stable isotope composition and hydrothermal fluids origin of uranium deposits in southern Zhuguang pluton. *Uranium Geol* 31:65–72 **(in Chinese with English abstract)**
- Mamyrin BA, Tolstikhin IN (1984) Helium isotopes in nature. Elsevier, Amsterdam, pp 1–248 **(in Chinese with English abstract)**
- Mao JW, Wang YT, Li HM, Pirajno F, Zhang CQ, Wang RT (2008) The relationship of mantle-derived fluids to gold metallogenesis in the Jiaodong Peninsula: evidence from D–O–C–S isotope systematics. *Ore Geol Rev* 33:361–381
- Mao JW, Xiong BK, Liu J, Pirajno F, Cheng YB, Ye HS, Song SW, Dai P (2017) Molybdenite Re/Os dating, zircon U–Pb age and geochemistry of granitoids in the Yangchuling porphyry W–Mo deposit (Jiangnan tungsten ore belt), China: implications for petrogenesis, mineralization and geodynamic setting. *Lithos* 286–287:35–52
- McLennan SM, Taylor SR (1979) Rare earth element mobility associated with uranium mineralization. *Nature* 282:247–250
- Mei JM (2000) Chemical typomorphic characteristic of pyrites from Zhilintou gold deposit, Suichang, Zhejiang. *Geoscience* 14:51–55 **(in Chinese with English abstract)**
- Ouyang PN, Wang QL (2013) Analysis of uranium mineralization conditions in Xiucaidong area, Rucheng, Hunan Province. *Geol Rev* 59:837–838 **(in Chinese)**

- Qin JN, Liu HB, He CM, Fei TW, Yan XL (2003) Characteristics of tectonic-geochemistry in the metallogenic fault and its prospecting potential in Huanggao district, Lujing uranium ore field. *J E Chin Geol Inst* 26:254–258 **(in Chinese with English abstract)**
- Seal RR (2006) Sulfur isotope geochemistry of sulfide minerals. *Rev Miner Geochem* 61(1):633–677
- Shao F, Zhu YG, Guo HS, He XM, Shao S (2010) Analysis on geological characteristics of uranium metallization and prospecting potential in Lujing orefield. *Uranium Geol* 26:295–300 **(in Chinese with English abstract)**
- Simmons SF, Sawkins FJ, Schlutter DJ (1987) Mantle-derived helium in two Peruvian hydrothermal ore deposits. *Nature* 329:429–432
- Stuart FM, Burnard PG, Taylor REA, Turner G (1995) Resolving mantle and crustal contribution to ancient hydrothermal fluids, He–Ar isotopes in fluid inclusions from Dae Hwa W–Mo mineralization, South Korea. *Geochim Cosmochim Acta* 59:4663–4673
- Sun SS, McDonough WF (1989) Chemical and isotopic systematics of oceanic basalts: implications for mantle composition and processes. *Geol Soc Lond Spec Publ* 42:313–345
- Ulrich T, Long DGF, Kamber BS, Whitehouse MJ (2011) In situ trace element and sulfur isotope analysis of pyrite in a paleoproterozoic gold placer deposit, Pardo and Clement Townships, Ontario, Canada. *Econ Geol* 106(4):667–686
- Wang J, Du LT (1995) Gas reduction: an important factor in the formation of uranium deposits. *Uranium Geol* 11(1):19–24 **(in Chinese with English abstract)**
- Wang MT, Luo Y, Sun ZF, Zhu JC, Li JH (1999) Discussion on genesis of uranium deposits in Zhuguang uranium metallogenic region. *Uranium Geol* 15(5):279–285 **(in Chinese with English abstract)**
- Wang AD, Wan JJ, Liu L, Hu FP, Zhang XF, Lai XD, Ding N (2015) Integrated SEM-EDS and XRD analyses for Huoqiu BIF and their geological implications. *J E Chin Inst Technol Nat Sci Ed* 38:23–31 **(in Chinese with English abstract)**
- Wang QL, Wang T, Ouyang PN, Li R (2016) Uranium enrichment regularity and next prospecting direction in Zhongshan area, SW, Lujing ore field. *Resour Inf Eng* 31:51–52 **(in Chinese)**
- Wang QL, Jiang HG, Ouyang PN, Zhang Y (2017) Analysis on geological feature of uranium mineralization and prospecting potential in Zhongshan area of Middle Zhuguangshan. *Uranium Geol* 33(01):16–21 **(in Chinese with English abstract)**
- Weaver BL, Wood DA, Tarney J, Joron JL (1987) Geochemistry of ocean island basalts from the south Atlantic: Ascension, Bouvet, St. Helena, Gough and Tristan da Cunha. *Geol Soc Lond Spec Publ* 30:253–267
- Xie GQ, Mao JW, Li W, Zhu QQ, Liu HB, Jia GH, Li YH, Li JJ, Zhang J (2016) Different proportion of mantle-derived noble gases in the Cu–Fe and Fe skarn deposits: He–Ar isotopic constraint in the Edong district, Eastern China. *Ore Geol Rev* 72:343–354
- Xiong YL, Zhai YS (1991) The mobility of rare-earth elements during hydrothermal activity: a review. *Chin J Geochem* 10(4):295–306
- Xu YC (1996) The mantle noble gas of natural gases. *Earth Sci Front* 3:63–71 **(in Chinese with English abstract)**
- Xu GF, Shao JL (1980) Typomorphic characteristics and practical significance of pyrite. *Geol Rev* 26:541–546 **(in Chinese)**
- Yan YT, Li SR, Jia BJ, Zhang N, Yan LN (2012) Composition typomorphic characteristics and statistic analysis of pyrite in gold deposits of different genetic types. *Earth Sci Front* 19:214–226 **(in Chinese with English abstract)**
- Zhang GQ, Hu RZ, Jiang GH, Liu S, Zhu WG, Tian JJ, Shuang Y, Fan XR (2010) Mantle-derived volatile components involved in uranium mineralization: evidence from He isotopes of the No. 302 uranium deposit. *Geochimica* 39(4):386–395 **(in Chinese with English abstract)**
- Zhang JD, Li ZY, Cai YQ, Guo QY, Li YL, Han CQ (2012) The main advance and achievements in the potential evaluation of uranium resource in China. *Uranium Geol* 28(6):321–326 **(in Chinese with English abstract)**
- Zhang J, Deng J, Chen HY, Yang LQ, Cooke D, Danyushevsky L, Gong QJ (2014a) LA–ICP–MS trace element analysis of pyrite from the Chang’an gold deposit, Sanjiang region, China: implication for ore-forming process. *Gondw Res* 26(2):557–575
- Zhang SG, Yuan Y, Yao CX (2014b) Petrology and ore-control of Zhuguangshan composite granitic pluton in middle section of Nanling region. *Chin J Nonferr Met* 24:1585–1598 **(in Chinese with English abstract)**
- Zhao FM, Shen CQ (1986) Experimental researches on paragenetic condition for pyrite and pitchblende and its role in pitchblende formation. *Uranium Geol* 2:193–199 **(in Chinese with English abstract)**
- Zheng YY, Gao SB, Zhang DQ, Zhang GY, Ma GT, Cheng SB (2006) Ore-forming fluid controlling mineralization in Qulong super-large porphyry copper deposit, Tibet. *Earth Sci* 31:349–354 **(in Chinese with English abstract)**
- Zong KQ, Klemd R, Yuan Y, He ZY, Guo JL, Shi XL, Liu YS, Hu ZC, Zhang ZM (2017) The assembly of Rodinia: The correlation of early Neoproterozoic (ca. 900 Ma) high-grade metamorphism and continental arc formation in the southern Beishan Orogen, southern Central Asian Orogenic Belt (CAOB). *Prec Res* 290:32–48
- Zou ML, Huang HY, Liu XY, Fan LT, Xiang TF, Xu H, Ouyang PN (2017) Characteristics of arsenic-bearing pyrite in the middle part of Zhuguang intrusion in South China and its relationship with uranium mineralization. *Geol Rev* 63(4):1021–1039 **(in Chinese with English abstract)**